# DESIGN AND TESTING OF BIONIC WINGED DEEP-LOOSENING SHOVEL FOR A STRIP TILLAGE DEEP-LOOSENING FERTILIZATION MACHINE

1

## 条带少耕深松施肥机带翼式深松铲仿生铲翼设计与试验

Shi-cheng XU¹); Gui-xiang TAO\*¹); Shu-juan YI¹); Song WANG¹); Yu-hang SAN¹)
College of Engineering, Heilongjiang Bayi Agricultural University, Daqing/P. R. China
Tel: +86-459-13836961877; E-mile: 15628820228@163.COM;
Corresponding author: Gui-xiang TAO
DOI: https://doi.org/10.35633/inmateh-77-45

Keywords: strip tillage; winged deep-loosening shovel; bionic design; tillage resistance

#### **ABSTRACT**

To address the issues of high operating resistance and insufficient soil-loosening performance encountered by winged deep-loosening shovels in strip-tillage fertilization machines, a bionic optimization design for the shovel wing was carried out based on a medium-sized winged deep-loosening shovel. A mechanical contact model between the shovel wing and soil was established to analyze the forces acting on the wing and the soil above it, as well as the soil disturbance characteristics induced by the wing. Following the principles of bionics, the head morphology of the hammerhead shark was extracted and used to derive a characteristic geometric equation, which was then applied to the bionic redesign of the shovel wing. Using discrete element simulation technology, a deep-loosening shovel-soil interaction model was constructed. Comparative experiments on wings of different shapes showed that the bionic-optimized wing reduces operating resistance and increases soil disturbance area compared with the conventional wing. Simulation results indicated that the bionic wing achieved an average soil disturbance area of 1635.63 cm² and an average operating resistance of 1143.76 N. Finally, bench validation tests were conducted, demonstrating an average actual soil disturbance area of 1648.20 cm² and an average actual operating resistance of 1102.01 N, results which fall within the allowable error range. Therefore, the bionic shovel wing meets the operational requirements.

#### 摘要

针对于条带少耕施肥机带翼式深松铲作业时作业阻力大、铲翼对土壤的松动效果不明显等问题,基于中型带翼式深松铲进行铲翼仿生优化设计。建立了铲翼与土壤间的力学接触模型,分析铲翼以及铲翼上方土壤受力情况,分析铲翼对土壤的扰动情况。应用仿生学原理,对双髻鲨头部特征进行提取,得出头部特征方程,根据特征方程进行铲翼仿生设计。应用离散元仿真技术,建立了深松铲-土壤仿真模型,通过对不同形状铲翼作业效果对比试验,确定了仿生优化后的铲翼相较于普通形状铲翼可以降低作业阻力增大土壤扰动面积。试验结果表明:仿生铲翼土壤扰动面积仿真平均值为1635.63cm²,作业阻力仿真平均值为1143.76N。最后进行台架验证试验,台架验证试验表明:仿生铲翼实际土壤扰动面积平均值为1648.20cm²,实际作业阻力平均值为1102.01N,满足数据误差范围,仿生铲翼符合作业要求。

#### INTRODUCTION

Compared with conventional tillage practices, reduced tillage with deep loosening can more effectively improve soil structure, enhance soil water retention capacity, and promote crop root development (He et al., 2018). This tillage approach has become increasingly important in modern sustainable agricultural systems (Qi et al., 2022). During reduced-tillage deep-loosening operations, the winged deep-loosening shovel expands the loosening range in the subsoil through its specialized wing structure, thereby improving tillage efficiency and serving as a key component in high-efficiency deep-loosening machinery. However, the existing wing designs of conventional deep-loosening shovels are no longer fully compatible with the performance requirements of modern agricultural production.

Issues such as high working resistance, increased energy consumption, and inadequate soil disturbance severely constrain the machinery's performance, making it difficult to satisfy the requirements of conservation tillage and precision, high-efficiency agriculture.

<sup>&</sup>lt;sup>1</sup> Shi-cheng Xu, Ms.; Gui-xiang Tao, Prof. Ph.D.; Shu-juan Yi, Prof. Ph.D.; Song Wang, Ph.D.; Yu-hang San, Ms.

Bionics has been widely applied in the field of agricultural engineering (Jia et al., 2017). For example, Zhao et al. (2022) analyzed the characteristic contours of dolphin pectoral and dorsal fins and, based on bionic design principles, developed a coupled mathematical model to determine optimal drag-reduction parameters for a dolphin-inspired deep-loosening shovel. Chen et al. (2024) extracted morphological features from the shark dorsal fin and incorporated them into a bionic dorsal-fin shovel design, demonstrating that the addition of a dorsal fin structure can effectively break through the plough pan and reduce tillage resistance. In addition, Jia et al. (2020) proposed a bionic design method for core-plough-type furrow openers by drawing inspiration from the efficient, low-resistance penetration structure of the badger's canine tooth surface, thereby reducing excessive operating resistance. Comparative tests demonstrated that, at identical operating speeds, the resistance of each optimized sliding furrow opener was lower than that of the standard core-plough-type furrow opener. Xu et al. (2025), drawing inspiration from the claws of badgers and the scales of pangolins, designed a coupled bionic deep-tillage implement. Simulation results showed that, across various operating speeds, the coupled bionic deep-tillage machine reduced operating resistance by 7.70%-16.02% compared with standard deep-tillage equipment. Zhang et al. (2024) applied the contour fitting characteristics of mole cricket foreleg tarsal segments to the structural design of deep-loosening shovels using bionic principles. Simulations comparing conventional and bionic deep-loosening shovels demonstrated that the bionic design provided superior drag-reduction and energy-saving performance. Son et al. (2022) developed a mathematical model to analyze the forces acting on mole claws during soil excavation, and then designed a bionic deep-loosening implement by integrating the claw morphology into a conventional deep-loosening structure. The ploughshare fragmentation and stress distribution of the deep-loosening component were simulated using EDEM and subsequently verified through soil bin and field tests. The results demonstrated that the bionic deep-loosening implement effectively enhanced soil fragmentation performance, with increased disturbance width leading to improved deep-loosening efficiency. Francisco et al. (2024) designed a deep-loosening shovel based on the inner and outer contour profiles of the Mexican ground squirrel's paw, employed computational fluid dynamics methods for structural analysis, and conducted tillage resistance tests to evaluate performance. The test results showed that the bionic deep-loosening shovel significantly reduced tillage resistance during operation. Tesliuk et al. (2019) proposed a methodology for developing soil-engaging tools inspired by the morphological characteristics of marine organisms. They emphasized that, under low-compaction soil conditions, effective soil disruption should be achieved through streamlined sliding penetration rather than traditional cutting-based fragmentation. Benard et al. (2010) applied the concept of non-smooth surface structures observed in burrowing animals to disc plough design to reduce soil resistance. Experimental results confirmed that incorporating bionic non-smooth surface units into disc ploughs can effectively decrease tillage resistance.

Existing research has not yet addressed the bionic optimization of shovel wings in winged deep-loosening shovels. Conventional shovel wing structures show limited effectiveness in reducing tillage resistance and increasing the soil disturbance area. As one of the primary soil-engaging components in winged deep-loosening tools, the high operating resistance of the shovel wing has long constrained improvements in tillage efficiency. Meanwhile, the penetration and soil-disturbance characteristics of the shovel wing play a critical role in determining the quality of deep loosening. Although previous studies have attempted to alleviate these issues through structural parameter adjustments or the use of new materials, challenges remain in achieving both resistance reduction and enhanced soil penetration under complex and variable soil conditions. Therefore, building upon a medium-sized winged deep-loosening shovel, this study applies bionic design principles to perform an optimized bionic redesign of the shovel wing. Using discrete element simulation (DEM) techniques, comparative analyses of shovel wings with different profile geometries were conducted. The performance of the bionic wing was further validated through bench tests, confirming the effectiveness and feasibility of the proposed bionic wing design.

## MATERIALS AND METHODS

#### Structure and working principle

The winged deep-loosening shovel consists of three main components: the shovel tip, shovel shank, and shovel wing. The shovel tip, mounted on the connecting frame of the deep-loosening mechanism, is positioned at a specific penetration angle at the leading end of the tool. It is the first part to enter the soil and is responsible for breaking through compacted soil layers. The shovel shank connects the shovel tip to the shovel wing, providing structural support. The buried portion of the shank contributes to soil loosening and bears most of the bending and tensile stresses during operation while transmitting traction forces to both the

shovel tip and shovel wing. Located behind the shovel tip, the shovel wing further loosens the soil following initial penetration and effectively disrupts the plough pan. The structure of the winged deep-loosening shovel and its shovel wing is shown in Fig. 1.

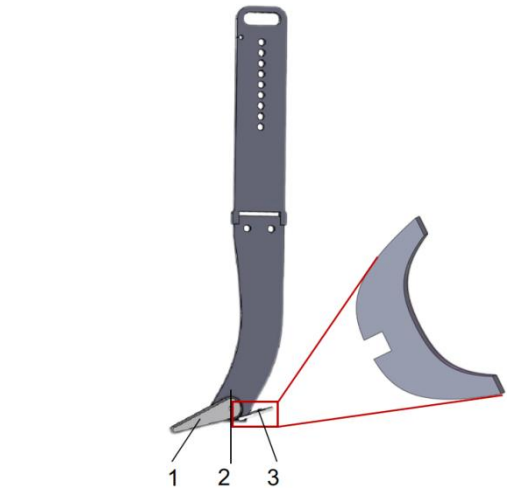


Fig. 1 – Winged deep-loosening shovel and shovel wing structure
1. Shovel tip; 2. Shovel shank; 3. Shovel wing

During deep-loosening operations, the deep-loosening shovel penetrates the soil and advances forward, with the shovel wing positioned behind the lower plane of the shovel tip. Due to its relatively large width, the shovel wing increases the lateral contact area with the soil and applies lateral forces to the surrounding soil particles, thereby enhancing horizontal soil disturbance. As a result, soil particles are subjected to both vertical and lateral shear forces, producing a multi-directional soil-loosening effect. This combined loading more effectively breaks down soil aggregates, fractures large clods into smaller particles, and disrupts compacted soil layers. In the black soil regions of Northeast China, long-term cultivation has led to the formation of a compacted plough pan layer. The shovel wing is particularly effective in breaking through this plough pan, facilitating smoother soil deformation and movement, and thereby improving deep-loosening efficiency.

#### Mechanical Analysis of Forces Acting on the Shovel Wing During Deep Loosening

The winged deep-loosening shovel is installed at a specific angle behind the lower plane of the shovel tip. During operation, the shovel wing engages the soil at an inclined angle, promoting lateral soil fragmentation. To analyze the forces acting on the shovel wing and the soil located above it during deep-loosening, the shovel wing can be simplified as an inclined plane subjected to soil forces, as shown in Fig. 2.

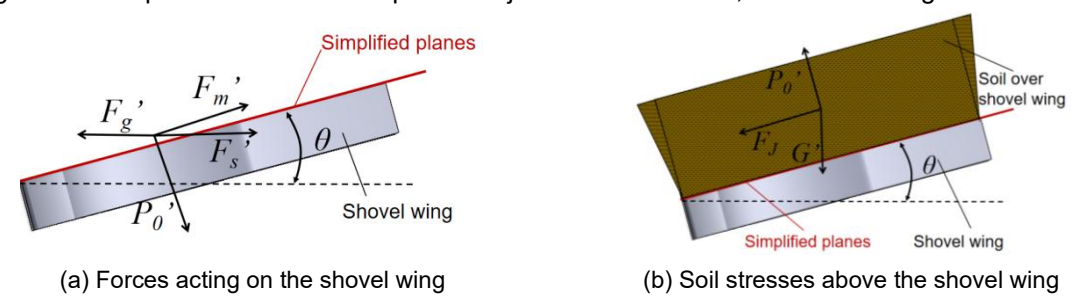


Fig. 2 - Force diagram of the shovel wing and the soil above it

The force balance equation for the shovel wing can be expressed according to Fig. 2(a):

$$F_{q}' = P_{0}' \sin \theta + F_{m}' \cos \alpha \theta + F_{s}' \tag{1}$$

where:  $F_q'$  is the traction force, N;  $P_{\theta'}$  is the normal load acting on the shovel wing, N;  $\theta$  is the inclination angle of shovel wing, (°);  $F_{m'}$  is the friction force exerted by the soil on the upper surface of the shovel wing  $F_{m'}=P_{\theta'}\beta_{1'}$ , N;  $F_{s'}$  is the cutting resistance acting on the shovel wing, N;  $\beta_{1'}$  is the friction coefficient between the soil and the shovel wing.

During deep-loosening operations, the likelihood of the shovel wing encountering hard stones or other rigid obstructions is relatively low. Therefore, the cutting resistance acting on the shovel wing can be considered negligible (Ma, 2022). According to Equation (1), the traction force is primarily influenced by the normal load exerted by the soil on the shovel wing, the friction coefficient between the soil and the shovel wing, and the inclination angle of the wing. The traction force and the horizontal operating resistance form a force balance. Consequently, the horizontal tillage resistance of the shovel wing is directly related to the normal load applied by the soil, the soil-wing friction coefficient, the wing inclination angle, and the effective working length of the wing.

To further investigate the shear disturbance and loosening effect of the shovel wing on the soil, a mechanical analysis was performed on the soil subjected to the action of the shovel wing. The force distribution is shown in Fig. 2(b).

According to the Mohr-Coulomb failure criterion, the shear strength of the soil can be expressed as:

$$\tau = F_d + \sigma \tan \varpi \tag{2}$$

where:  $\tau$  is the soil shear strength, kPa;  $\sigma$  is the soil normal stress, kPa.

According to Fig. 2(b), the normal and shear stresses of the soil acting on the shovel wing are:

$$\tau' = \frac{F_J}{S_1} \tag{3}$$

$$\tau' = \frac{F_J}{S_1}$$

$$\sigma' = \frac{P_0'}{S_1}$$
(3)

where:  $\tau'$  is the shear stress on the soil, kPa;  $F_J$  is the shear force acting on the soil along the surface of the shovel wing, N;  $\sigma'$  is the normal stress on the soil, kPa;  $S_I$  is the contact area between the soil and the shovel wing, mm<sup>2</sup>.

When the shear stress exerted by the shovel wing on the soil exceeds the soil's shear strength, shear failure occurs. Combining Eqs. (2), (3), and (4), the critical condition for soil shear failure can be expressed as:

$$F_I \ge F_d S_1 + P_0 ' \tan \varpi$$
 (5)

As indicated by Equation (5), soil shear failure is influenced by soil cohesion, contact area, and internal friction angle. Since inherent soil parameters (e.g., cohesion and internal friction angle) are generally uncontrollable, the key factor affecting shear failure effectiveness is the contact area between the shovel wing and the soil. Increasing the width of the shovel wing increases the contact area. Combined with Equation (1), it is evident that, under identical working speeds and tillage depths, the primary structural parameters affecting the performance of the winged deep-loosening shovel are the shovel wing angle, the wing width, and the wing profile. Based on simulation modeling and experimental testing conducted in this study, the optimal shovel wing angle was determined to be 28°.

#### Bionic shovel winged design

Research by Li et al. (2018) indicates that the winged deep-loosening shovel can produce more than twice the soil disturbance of a non-winged deep-loosening shovel, demonstrating that the shovel wing plays a crucial role in achieving effective deep loosening. The shovel wing directly influences both soil disturbance and tillage resistance, and its geometric shape and structural configuration are therefore key design parameters. Increasing the wing width enhances lateral contact with the soil, thereby expanding the soil disturbance area. However, a greater wing width also increases tillage resistance. In deep-loosening operations, lower tillage resistance reduces traction demand and energy consumption of the power unit. Therefore, shovel wing design must balance two objectives: decreasing tillage resistance while maintaining sufficient soil disturbance. To meet these requirements, it is necessary to conduct in-depth research on the shape and structural characteristics of the shovel wing. The application of bionic design principles to shovel wing optimization provides a promising approach, enabling the realization of both reduced tillage resistance and effective soil disturbance.

#### **Biomimetic Prototype Selection**

The hammerhead shark is a distinctive marine species characterized by a uniquely broad and laterally expanded, hammer-shaped head. The most prominent feature of the hammerhead shark is its broad, flattened head, which exhibits streamlined characteristics extending laterally. This unique head structure is unparalleled among sharks. The hammerhead shark's distinctive head shape enables it to increase the surface area of its head that disturbs water flow while swimming. This reduces hydrodynamic drag on its body. Furthermore, due to its streamlined head, the additional drag incurred does not significantly increase, thereby enhancing overall swimming efficiency. This allows it to swim rapidly through water and improves its ability to capture the prey (*Gong et al., 2021*). Drawing from this biomimetic inspiration, the broad and flattened head of the hammerhead shark was selected as the biological prototype for shovel wing design. By incorporating the shark's streamlined and laterally extended geometry, the biomimetic shovel wing can increase the soil disturbance area during deep loosening while avoiding a substantial increase in tillage resistance.

The hammerhead shark's head enhances its swimming efficiency. Its head extends laterally on both sides, forming a broad, hammer-like shape. The external morphology and head characteristics of the hammerhead shark are shown in Fig. 3. From a biomimetic engineering perspective, extracting and applying the geometric features of the hammerhead shark's head provides a basis for designing the shovel wing profile of the winged deep-loosening shovel.

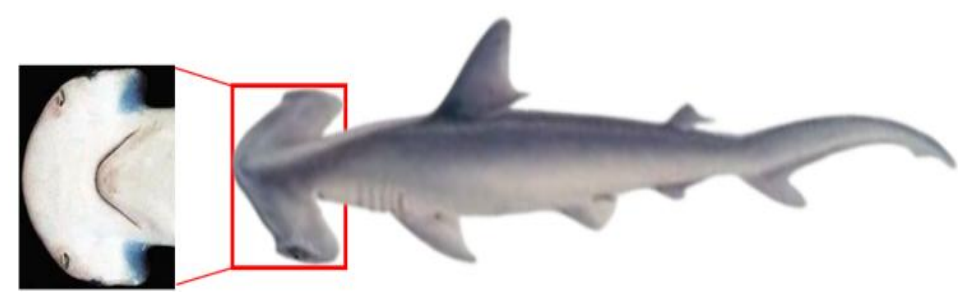


Fig. 3 – Schematic diagram of the hammerhead shark's body structure and head characteristics

#### Hammerhead Shark Head Feature Extraction

Based on the theoretical framework of reverse engineering (*Hu et al., 2019*), this study performs precise extraction and fitting of the head (head) features of the hammerhead shark. MATLAB 2020b was used to obtain the boundary profile, and the extraction process is shown in Fig. 4. First, the original image was converted to grayscale and then binarized. The Canny edge detection algorithm was applied to extract the boundary contour of the head. Due to the presence of eyes and mouth opening, the extracted profile exhibits local irregularities. However, the biomimetic shovel wing requires a smooth and continuous surface geometry; therefore, the raw boundary curve was smoothed to eliminate discontinuities and sharp fluctuations. The coordinates of the resulting smoothed contour were then exported for subsequent fitting and parametric modeling.

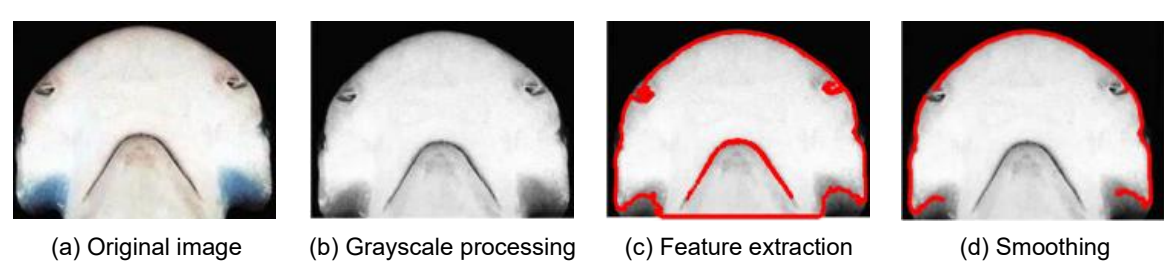


Fig. 4 - Extraction process of the hammerhead shark head boundary

Curve fitting was carried out on the smoothed boundary profile to obtain the fitted head curve and its corresponding mathematical expression. To ensure high fitting accuracy, three fitting methods were applied, and the coefficient of determination was used as the evaluation metric to identify the optimal fitting approach. Using MATLAB 2020b, the boundary contour was fitted using polynomial fitting, exponential function fitting, and rational function fitting. The resulting fitted curves are shown in Fig. 5.

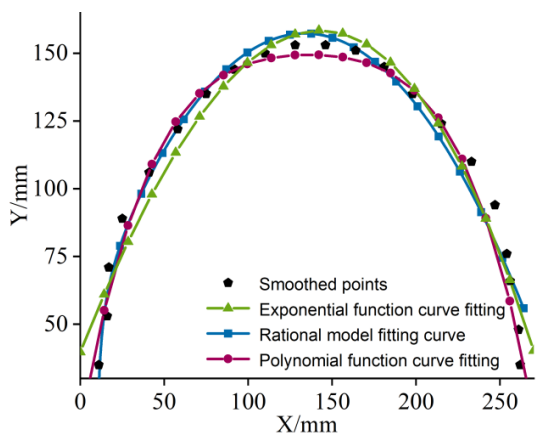


Fig. 5 - Hammerhead shark head boundary extraction process

The fitted equations and their corresponding coefficients of determination are listed in Table 1. The coefficient of determination for the exponential fit was 0.9542, that for the rational function fit was 0.9638, and the polynomial fitting method achieved the highest value at 0.9795. Therefore, the polynomial model was selected as the optimal fitting approach for representing the hammerhead shark head characteristic curve.

Fitting methods and their coefficients of determination

Table 1

Method	Fitted equation	equation Coefficient of determination	
Exponential function	y=-1386.6377e <sup>0.002559x</sup> +5.1157x+	0.954	
	1426.3329		
Polynomial function	y=-0.000000285x <sup>4</sup> +0.0001545x <sup>3</sup> -	0.979	
	0.0336x <sup>2</sup> +3.4351x+12.6281		
Rational model	y=(-0.006+1.629x+40.546x <sup>2</sup> )/(1-	0.963	
	554.639x)		

A biomimetic shovel wing was designed by fitting a curve equation derived from the head characteristics of the hammerhead shark. The 3D model of the biomimetic shovel wing was constructed in SolidWorks 2023. The outer contour of the wing was generated using the equation-driven curve function, after which the surface was extruded and trimmed to form the mounting interface. The resulting biomimetic shovel wing model is shown in Fig. 6.



Fig. 6 – Structure of the biomimetic shovel wing model

#### Simulation comparison experiments

In the previous section, the external geometry of the biomimetic shovel wing was established by fitting the hammerhead shark head contour. To verify the operational advantages of the biomimetic shovel wing over conventional wing geometries, comparative deep-loosening performance evaluations were conducted. To minimize experimental cost and shorten the development cycle, the discrete element method (DEM) was used to simulate the deep-loosening process. Currently, conventional shovel wing designs are predominantly rectangular or triangular in form. Therefore, three shovel wing configurations were selected for comparative simulation to evaluate their operational performance.

### Simulation model establishment

This study developed a biomimetic deep-loosening shovel to address the problems of insufficient soil disturbance and high tillage resistance encountered in reduced-tillage deep-loosening and fertilization operations.

The proposed design provides an optimized solution for improving operational efficiency and reducing energy consumption. Since the reduced-tillage deep-loosening fertilization machine is primarily used in the typical black soil region of Northeast China, the performance evaluation conducted in this study is limited to this soil type. Other black soil conditions were not considered and will require further validation in future research.

As normal arable land contains few stones or other hard objects, no stones were encountered during actual soil sampling. During deep loosening operations, when the deep loosening shovel encounters stones, these are typically forced to the sides, causing no significant impact on the loosening effect. Therefore, stones in the soil are not considered when establishing the soil model. Initially, representative black soil samples were collected from Daqing Farm in Wudalianchi City, Heilongjiang Province. Subsequently, characteristic parameters were determined for these representative black soil samples to establish a soil particle model based on the measured parameters. Using EDEM 2022 software, a soil channel was constructed. Based on the measured soil parameters, a soil model was established. Different particle diameters were set according to the measured particle size distribution of the soil samples and mixed to create a soil particle bed for simulating restored conventionally tilled soil. The soil particle bed is shown in Figure 7.

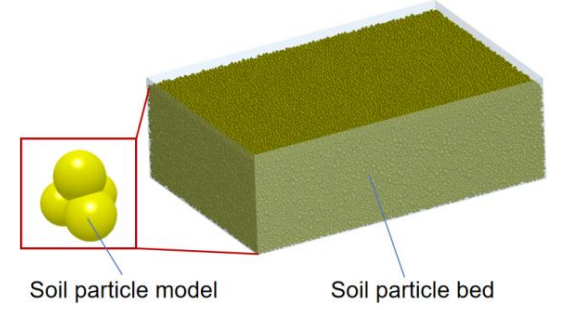


Fig. 7 - Soil particle model and soil particle bed diagram

Based on the hammerhead shark head characteristic curve obtained above, a biomimetic shovel wing model was constructed. For comparison, rectangular and triangular shovel wings with the same width and length as the biomimetic wing were also designed. All three shovel wing types were installed at the same mounting angle behind the cutting edge of an identical deep-loosening shovel body. The three shovel models were then imported into EDEM 2022 in .slt format. In EDEM 2022, the shovel wings were assigned material properties corresponding to 65 Mn steel, with a density of 7850 kg/m³, Poisson's ratio of 0.3, and shear modulus of 7.8×10<sup>10</sup> Pa. The contact model and parameter settings were kept consistent across all shovel wing types.

The three deep-loosening shovel models were combined with a soil particle bed and simulated using the Hertz-Mindlin with JKR contact model, which more accurately represents cohesive behavior in soil (Zang et al., 2022). Based on agronomic requirements and the depth of the plow pan, the optimal tillage depth was set to 320 mm, which ensures effective plow pan disruption while satisfying cultivation needs. The implement utilizes a hydraulic depth-control system to maintain a consistent working depth during operation. After configuring the simulation environment and parameters, three deep-loosening operation models corresponding to the biomimetic, rectangular, and triangular shovel wings were obtained, as shown in Fig. 8. The specific simulation parameters are listed in Table 2.

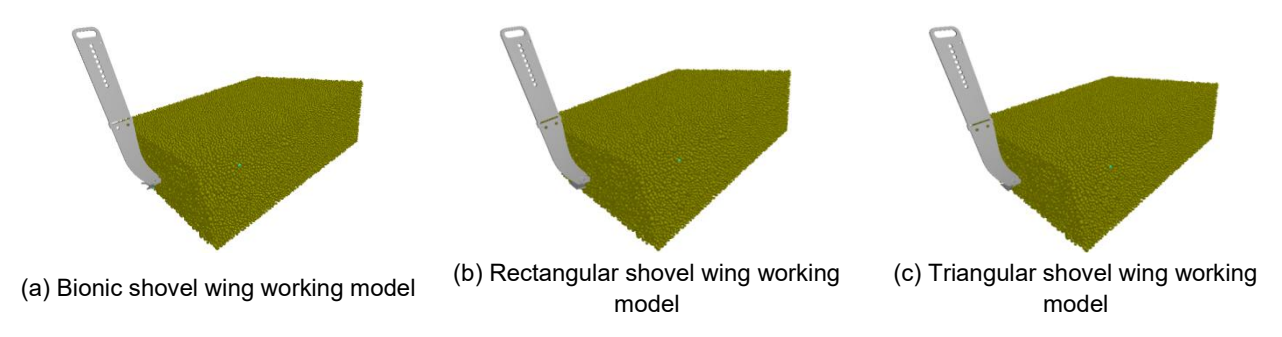


Fig. 8 – Deep-loosening soil operation models for the biomimetic, rectangular, and triangular shovel wings

Table 2

Simulation test parameters

Parameter	Value	Parameter	Value
Poisson's ratio of soil particles	0.30	Particle-65 steel dynamic friction coefficient	0.15
Soil density (kg/m³)	1600	Poisson's ratio of 65 steel	0.35
Soil particle shear modulus (Pa)	1×107	Density of 65 steel (kg/m³)	7850
Particle-particle coefficient of restitution	0.3	65 steel shear modulus (Pa)	7.8×1010
Particle-particle static friction coefficient	0.7	Soil particle bed thickness (mm)	450
Particle-particle kinetic friction	0.2	Horizontal speed of deep loosening shovel (m/s)	1.5
Particle-65 steel coefficient of restitution	0.35	Tillage depth (mm)	320
Particle-65 steel static friction coefficient	0.6	Grid size (mm)	24

#### Simulation experiment design

Deep-loosening simulation experiments were carried out in EDEM 2022, using tillage resistance and soil disturbance area as performance evaluation indices. A lower tillage resistance combined with a larger soil disturbance area indicates improved operational efficiency and reduced energy consumption of the deep-loosening shovel. The objective of this experiment is to verify that the biomimetic shovel wing provides superior performance compared with conventional rectangular and triangular shovel wing configurations.

To accurately obtain tillage resistance values, three preliminary simulation trials were conducted. The reaction force acting on the shovel during operation was extracted at each simulation timestep using the post-processing tools in EDEM 2022. Subsequently, ORIGIN 2021 was used to plot the tillage resistance curves for the three trials. The resulting tillage resistance curves are shown in Fig. 9.

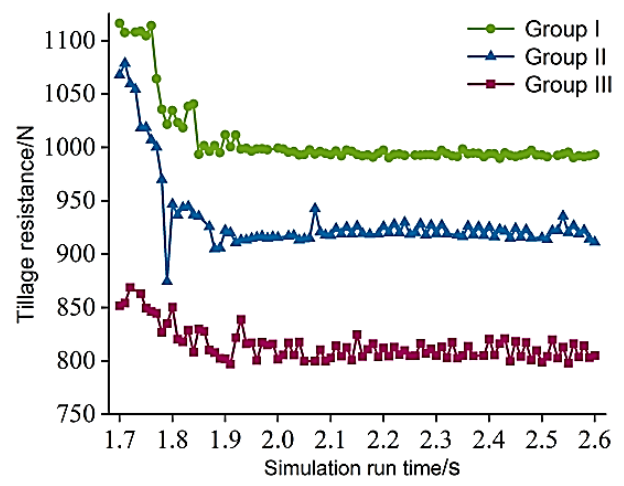


Fig. 9 - Tillage resistance line curves from three repeated simulation trials

As shown in Fig. 9, the tillage resistance of the deep-loosening shovel remains relatively stable within the time interval of 1.90-2.50 s. Therefore, the average tillage resistance was calculated over this period.

For soil disturbance analysis, a cross-sectional plane was taken 225 mm ahead of the shovel's vertical centerline at a simulation time of 2.3 s. A 30 mm slicing thickness was used to obtain the soil disturbance trench profile. The disturbance boundary was then identified and the boundary coordinates were imported into ORIGIN 2021 to generate the profile curve. The disturbed soil area was calculated using the integral absolute area method. The boundary selection and soil disturbance area computation process are illustrated in Fig. 10.

For the soil disturbance analysis, a cross-sectional plane was taken 225 mm ahead of the shovel's vertical centerline at a simulation time of 2.3 s. A slicing thickness of 30 mm was applied to obtain the soil disturbance trench profile. The disturbance boundary was then extracted, and the boundary coordinate data were imported into ORIGIN 2021 to generate the corresponding profile curve. The disturbed soil area was calculated using the integral absolute area method. The boundary extraction and soil disturbance area calculation process are illustrated in Fig. 10.

Table 3

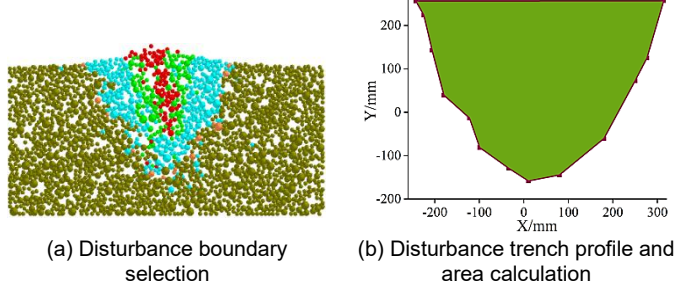


Fig. 10- Soil disturbance area calculation procedure

#### **RESULTS AND DISCUSSIONS**

Using EDEM 2022, comparative simulations were carried out to evaluate the deep-loosening performance of the three shovel wing configurations. The resulting tillage resistance curves and soil disturbance trench profiles for each shovel wing type are shown in Fig. 11.

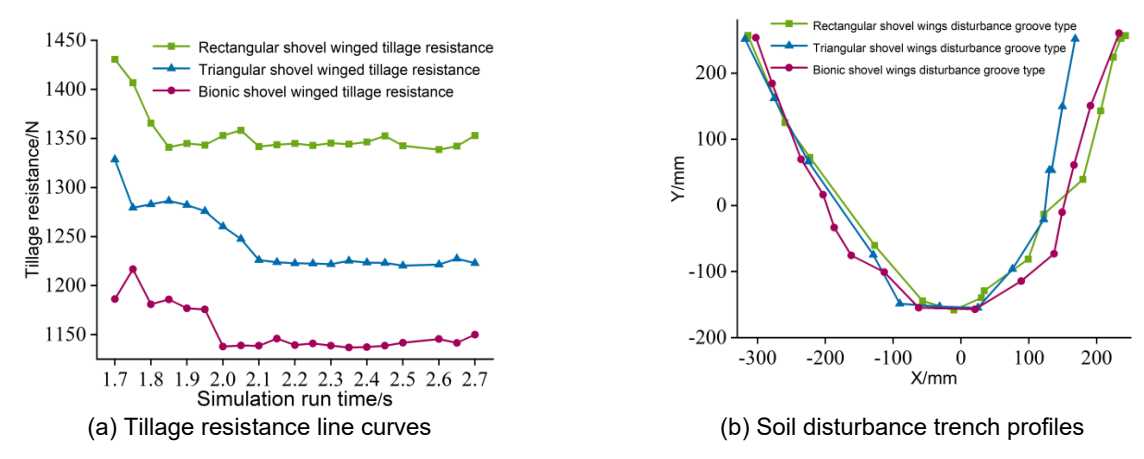


Fig. 11 - Comparison of the deep-loosening performance of the three shovel wing types

As shown in Fig. 11(a), the rectangular shovel wing exhibits the highest tillage resistance, followed by the triangular shovel wing, while the biomimetic shovel wing demonstrates the lowest resistance. This can be attributed to differences in soil flow behavior around the shovel wings. The rectangular wing presents a broad, flat contact surface that restricts the lateral movement of loosened soil, causing greater soil accumulation in front of the tool and increasing the horizontal resistance during forward motion. The triangular wing, with its inclined surface, allows soil to slide to some extent, thereby reducing tillage resistance relative to the rectangular wing; however, the fixed and relatively steep inclination still hinders smooth soil flow. In contrast, the biomimetic wing incorporates a streamlined head-inspired profile that promotes lateral soil deflection and flow on both sides of the wing, effectively reducing soil buildup and significantly lowering tillage resistance.

As shown in Fig. 11(b), the biomimetic shovel wing produces the largest soil disturbance area, followed by the rectangular wing, while the triangular wing results in the smallest disturbance. Under the condition of equal wing widths, the streamlined head-inspired geometry of the biomimetic wing increases the effective contact area with the soil and enhances lateral soil displacement, thereby expanding the disturbance zone. In addition, the smooth curvature of the biomimetic wing promotes more continuous soil flow during deep loosening, reducing soil blockage and further improving disturbance efficiency.

The average tillage resistance and soil disturbance area values for the three shovel wing types are summarized in Table 3.

Comparison of performance indicators for the three shovel wing types

 Shovel wing shape
 Soil disturbance area (cm²)
 Tillage resistance (N)

 Rectangular shovel wing
 1564.91
 1346.77

 Triangular shovel wing
 1435.76
 1241.79

 Bionic shovel wing
 1681.70
 1150.08

As shown in Table 3, compared with the rectangular shovel wing, the biomimetic shovel wing increases the soil disturbance area by 56.79 cm<sup>2</sup> and reduces tillage resistance by 196.69 N. Compared with the triangular shovel wing, it increases the soil disturbance area by 185.94 cm<sup>2</sup> and reduces tillage resistance by 91.71 N.

To reduce the influence of random variation, the deep-loosening simulation comparisons for the three shovel wing types were repeated three times. The results consistently showed that the rectangular shovel wing exhibited the highest tillage resistance, while the triangular shovel wing produced the smallest soil disturbance area. The biomimetic shovel wing demonstrated both the lowest tillage resistance and the largest soil disturbance area, indicating a clear operational advantage over the conventional designs. Across the repeated simulation trials, the biomimetic shovel wing achieved an average soil disturbance area of 1635.63 cm² and an average tillage resistance of 1143.76 N.

During deep-loosening operations, the implement must overcome tillage resistance while maintaining a forward travel speed. The required power can be calculated as:

$$K = \frac{Fv}{3600\eta} \tag{6}$$

Where: K is the required operating power, kw; F is the tillage resistance, N; v is the forward speed of the implement, km/h;  $\eta$  is the transmission system efficiency.

Calculations of operating power based on the measured tillage resistance and forward speed indicate that the biomimetic shovel wing can reduce the energy consumption of the deep-loosening implement by approximately 11%–18%.

In summary, the biomimetic shovel wing enhances the soil-penetration ability of the deep-loosening shovel and increases the soil disturbance area through its streamlined, biologically inspired profile. Compared with conventional shovel wing geometries, the biomimetic wing reduces tillage resistance while expanding the disturbed soil volume, thereby improving operational efficiency and reducing energy consumption. These results provide theoretical and technical support for improving the performance of deep-loosening shovels and offer a reference for further optimization and promotion of reduced-tillage deep-loosening equipment.

#### **Bench validation experiments**

To verify the consistency between the actual operational performance of the biomimetic shovel wing and the simulation results, a bench-scale verification test rig was designed and constructed. The test rig consisted of a soil tank, a deep-loosening assembly, a drive motor, and linear guide rails. To ensure that soil conditions in the bench tests closely matched those used in the simulations, representative black soil was collected from the field test area, transported to the laboratory, and compacted into the soil tank to achieve similar bulk density and moisture conditions. The structural layout of the verification test rig is shown in Figure 12.



Fig. 12–Structure of the bench verification test rig
1. Drive motor 2. Soil tank 3. Deep-loosening mechanism 4. Guide rails

The biomimetic shovel wing was fabricated according to the rendered three-dimensional model and mounted at a 28° angle behind the shovel tip of the deep-loosening blade. The assembled deep-loosening shovel was then installed onto the deep-loosening mechanism. The mechanism was connected to the guide rail via a mounting bracket, allowing controlled linear motion. During testing, the operating parameters of the bench system were set to a forward speed of 5 km/h and a deep-loosening depth of 320 mm. After parameter configuration, validation experiments were carried out and the corresponding data were recorded.

To quantify the actual soil disturbance area, trench profiles were recorded after the bench experiment. The soil disturbance profiles were extracted using MATLAB 2020b, and the resulting coordinate data were imported into ORIGIN 2021 to generate the trench profile curves and calculate the disturbed soil area. The resulting trench profile diagram is shown in Figure 13.

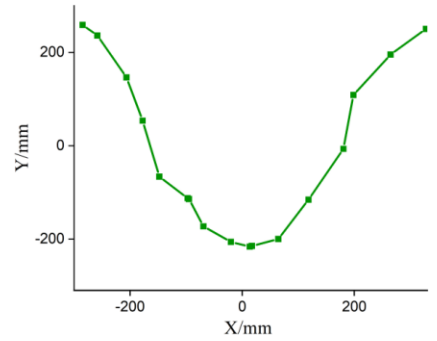


Fig. 13 - Trench profile obtained from the bench validation experiment

One end of the Keli PST force sensor was connected to the deep-loosening shovel, while the opposite end was fixed using a sliding counterweight. The force sensor was interfaced with a digital display unit, and the stabilized resistance values during operation were recorded via a data acquisition module on the host computer. The recorded data were subsequently exported for the calculation of tillage resistance. The resistance measurement setup is shown in Figure 14.



Fig. 14 - Resistance measurement device

1. Host computer display interface; 2. Digital resistance meter; 3. Keli PST Type Force Sensor

On 27 May 2025, three validation trials were carried out. After each trial, the soil surface was re-leveled to ensure consistent initial conditions across tests. The soil disturbance area for each trial was calculated in ORIGIN 2021 based on the extracted trench profile data. Tillage resistance data were obtained from the data acquisition module and processed to determine the corresponding resistance values. The results from the three validation trials are shown in Figure 15.

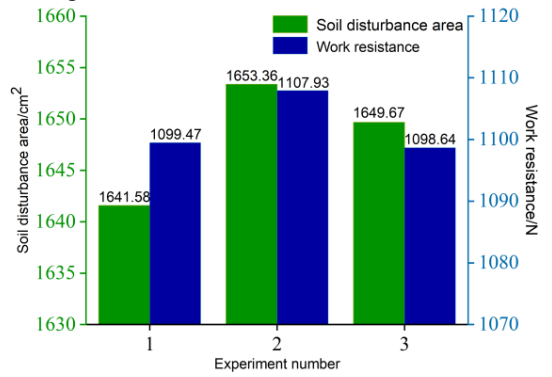


Fig. 15- Bar chart of experiment results

The soil disturbance areas for the three bench validation trials were 1641.58 cm², 1653.36 cm², and 1649.67 cm², with an average of 1648.20 cm². The corresponding tillage resistances were 1099.47 N, 1107.93 N, and 1098.64 N, yielding an average of 1102.01 N. Compared with the simulation results, the average soil disturbance area differed by 5.3 cm², and the average tillage resistance differed by 41.75 N.

The slightly larger soil disturbance area observed in the bench tests may be attributed to the lower precision in profile extraction compared with the controlled simulation environment. The reduced tillage resistance measured in the validation tests may be related to the presence of larger soil aggregates in the physical trials, which altered soil failure behavior relative to the particle-based simulation. Although minor deviations exist between the simulation and bench validation results, these differences fall within the acceptable experimental error range and do not affect the reliability of the overall research conclusions.

In summary, the actual deep-loosening performance of the biomimetic shovel was consistent with the simulation results. Compared with conventional winged deep-loosening shovels, the biomimetic design effectively reduced tillage resistance and increased the soil disturbance area during operation. This demonstrates that the biomimetic shovel wing provides an optimized solution for improving operational efficiency and reducing energy consumption in reduced-tillage deep-loosening fertilization equipment used in the typical black soil regions of Northeast China.

#### **CONCLUSIONS**

This study proposed a biomimetic optimization design for the winged deep-loosening shovel used in reduced-tillage fertilization operations in the typical black soil regions of Northeast China. The proposed design increases soil disturbance while reducing tillage resistance, thereby improving operational efficiency and lowering energy consumption.

A mechanical contact model between the shovel wing and soil was established, and the force transmission characteristics during deep-loosening operations were analyzed. The results clarified the influence of shovel-wing geometry on soil disturbance and tillage resistance. Based on the principles of bionic design, the characteristic curve of the hammerhead shark head was extracted and fitted to obtain a structural profile equation. This equation was used to develop the biomimetic shovel wing shape.

Using the discrete element method, a deep-loosening simulation model was constructed to compare the operational performance of the biomimetic shovel wing and conventional shovel wings. With tillage resistance and soil disturbance area as evaluation metrics, the biomimetic shovel wing demonstrated superior performance, achieving an average simulated soil disturbance area of 1635.63 cm² and an average simulated tillage resistance of 1143.76 N. Bench validation tests confirmed the simulation results. The biomimetic shovel wing yielded an average soil disturbance area of 1648.20 cm² and an average working resistance of 1102.01 N, both within the acceptable deviation range. This verifies that the biomimetic shovel wing meets practical operational requirements. Overall, the biomimetic shovel wing effectively reduces tillage resistance while enlarging the soil disturbance area.

#### **ACKNOWLEDGEMENT**

This paper was supported by the National Key Research and Development Program of China (2023YFD1501005-06) and the Heilongjiang Provincial Key Research and Development Program (2022ZX05B05-01).

### **REFERENCES**

- [1] Chen Q., Shan H., Wei C. & Zhang X. (2024). Simulation analysis of cultivation behavior of shark-fin-like deep loosening shovel based on discrete elements (基于离散元的仿鲨鱼鳍深松铲耕作行为仿真分析) [J]. *Journal of Chinese Agricultural Mechanization*, Vol. 45, Issue 12, pp. 15-20.
- [2] Chirende B., Li J., & Wen L. (2010). Effects of bionic non-smooth surface on reducing soil resistance to disc ploughing [J]. *Technological Sciences*, Vol. 53, pp. 2960-2965.
- [3] He j., Li H., Chen H., Lu C. & Wang Q. (2018). Research Progress of Conservation Tillage Technology and Machine (保护性耕作技术与机具研究进展) [J]. *Transactions of the Chinese Society for Agricultural Machinery*, Vol. 49, Issue 4, pp. 1-9.
- [4] Hu S. (2019). Personalized product innovation design and model making based on reverse engineering (基于逆向工程的个性化产品创新设计与模型制作) [J]. *Mechanical Engineering & Automation,* Issue 5, pp.197-199.
- [5] Jia H., Wang W., Chen Z., Zheng T., Zhang P., & Zhuang J. (2017). Research Status and Prospect of Soil-engaging Components Optimization for Agricultural Machinery (农业机械触土部件优化研究现状与展望) [J]. *Transactions of the Chinese Society for Agricultural Machinery*, Vol. 48, Issue 7, pp. 1-13.

- [6] Jia H., Meng F., Liu L., Shi S., Zhao J., & Zhuang J. (2020). Biomimetic Design and Experiment of Coreshare Furrow Opener (芯铧式开沟器仿生设计与试验) [J]. *Transactions of the Chinese Society for Agricultural Machinery*, Vol. 51, Issue 04, pp. 44-49+77.
- [7] Li B., Chen Y., & Chen J. (2018). Comparison of Two Subsoiler Designs Using the Discrete Element Method (DEM). *Transactions of the ASABE*, Vol. 61, Issue 5, pp. 1529-1537.
- [8] Márquez G.F., Reyes M.E., Morales M.C., Cantū L.R., Bello M.C., & Lorence A.G. (2024). Subsoiler Tool with Bio-Inspired Attack Edge for Reducing Draft Force during Soil Tillage [J]. *AgriEngineering*, Vol.6, Issue 3, pp. 2678-2693.
- [9] Ma C. (2022). Design and experiment of deep fertilization strip tillage device for corn in Northeast China (东北玉米区深施肥带状耕作装置设计与试验). *Chinese Academy of Agricultural Mechanization Sciences*.
- [10] Ma K., Zhang R., Guo X., Xu M., & Pu Y. (2021). Shape design and flow field characteristics of a robotic fish imitating the head of a hammerhead (仿双髻鲨头部的仿生机器鱼外型设计及其流场特性) [J]. *Chinese Journal of Theoretical and Applied Mechanics*, Vol. 53, Issue 12, pp. 3389-3398.
- [11] Qi Z., Song F., Zhang Z., Liu M., Yin Z., & Li A. (2022). Effects of Different Conservation Tillage Methods on Soil Hydrothermal Condition as well as Maize Yield in Cold Black Soil Region (保护性耕作对寒地黑土 土壤水热效应与玉米产量的影响) [J]. *Transactions of the Chinese Society for Agricultural Machinery*, Vol. 53, Issue 12, pp. 380-389.
- [12] Son W., Jiang X., LI L., & Jin T. (2022). Increasing the width of disturbance of plough pan with bionic inspired subsoilers [J]. Soil & Research, Vol. 220.
- [13] Tesliuk H., Volik B., Sokol S., & Ponomarenko N. (2019) Design of working bodies for tillage tools using the methods of bionics [J]. *Восточно-Европейский журнал передовых технологий*, Vol. 3, Issue 1, pp. 49-54.
- [14] Xu Z., Qi H., Wang L., Wang S., Liu X., & Ma Y. (2025) DEM Study and Field Experiments on Coupling Bionic Subsoilers [J]. *Biomimetics*, Vol. 10, Issue 5, pp. 306-306.
- [15] Zhao Y., Wang L., Niu W., Gao Z., Li P., Gao W., Fan Q., & Feng R. (2022). Analysis of Working Mechanism Based on Coupled Bionic Dolphin Subsoiling Shovel (基于耦合式仿生海豚深松铲的作业机理分析) [J]. South Forum, Vol. 53, Issue 22, pp. 1-4+22.
- [16] Zhang X., You Y., Wang D., Wang Z., Liao Y., & Lv J. (2022). Design and Experiment of Soil-breaking and Root-cutting Cutter Based on Discrete Element Method (基于离散元法的板结草地破土切根刀优化设计与试验) [J]. *Transactions of the Chinese Society for Agricultural Machinery*, Vol. 53, Issue 11, pp. 176-187.
- [17] Zhang L., Wang X., Chen J., Wang H., & Cao Y. (2024). Analysis and Optimization of Low-Resistance Animal Bionic Subsoiling Shovel Based on EDEM [J]. *Agriculture*, Vol. 14, Issue 11, pp. 2046-2046.